

# Ab initio study of nonadiabatic interactions in the photodissociation of ketene

Qiang Cui and Keiji Morokuma<sup>a)</sup>

Cherry L. Emerson Center for Scientific Computation and Department of Chemistry, Emory University, Atlanta, Georgia 30322

(Received 2 May 1997; accepted 26 June 1997)

*Ab initio* calculations have been carried out on potential-energy surfaces for the photodissociation of ketene.  $S_0$  and  $S_1$  state cross extensively around the Franck–Condon (F–C) region upon C–C–O bending, and the  $S_1 \rightarrow S_0$  internal conversion is expected to be very efficient.  $S_1$  and  $T_1$  stay close in energy in the F–C region, but do not couple strongly due to the small spin–orbit coupling, and direct  $S_1 \rightarrow T_1$  intersystem crossing is unlikely. The triplet state, which produces the ground-state products is likely to be formed via the process  $S_1 \rightarrow S_0 \rightarrow T_n$ .  $S_0$  crosses with the lowest triplet state ( $T_1$  or  $T_2$ ) at rather low energy near the triplet minimum. The  $S_0/T_n$  crossing persists all along the C–C dissociation pathway. As C–C is stretched, the energy of the crossing increases and the crossing structure deviates substantially from the reaction path. These results suggest that, if intersystem crossing at higher potential energy is favored, the rate of reaction may reflect the dynamics of intersystem crossing and that on the triplet surface. © 1997 American Institute of Physics. [S0021-9606(97)00937-9]

## I. INTRODUCTION

Determination and understanding of the detailed reaction mechanism and rate constant of reactions involving ketene have been the goal of numerous experimental as well as theoretical studies. The isomerization of carbon-labeled ketene has been studied by a series of fascinating experimental work by Moore and co-workers,<sup>1</sup> and theoretically by Miller and Gezelter.<sup>2</sup> The photodissociation of ketene into the singlet  $\text{CH}_2 + \text{CO}$  has also been studied in detail experimentally by Moore *et al.*<sup>3</sup> as well as Wodtke *et al.*,<sup>4</sup> and theoretically by Klippenstein and Marcus<sup>5</sup> using the variational Rice–Ramsperger–Kassel–Marcus (RRKM) theory. More recently, much attention has been focused on the photodissociation of ketene into the triplet  $\text{CH}_2 + \text{CO}$ . Kim, Lovejoy, and Moore<sup>6</sup> prepared rotational cold ketene on the  $S_0$  ground state ( $X^1A_1$ ) and used a UV laser to excite the molecule to the  $S_1$  singlet excited state ( $A^1A_2$ ), which then underwent intersystem crossing to the  $T_1$  triplet surface. The products,  $\text{CH}_2(^3B_1) + \text{CO}$ , were detected using laser-induced fluorescence (LIF) of the CO fragment. At first glance, the observed rate constants are very close to the prediction of the standard RRKM theory, and the energy dependence of the rate seems to exhibit a sharp stair function structure. However, upon closer inspection, they found that not all of the detailed fine structures in the rate constant could be explained using the standard RRKM.

Gezelter and Miller<sup>7</sup> recently carried out reduced-dimension quantum calculations (one-dimensional and two-dimensional ABC-DVR<sup>8</sup>) for the microcanonical rate constant, trying to solve this mystery. Even though the overall results agreed with experimental findings, the step function structure was washed out by tunneling through the thin barrier predicted by Allen and Schaefer<sup>9</sup> with *ab initio* calcula-

tions. To explain the discrepancies, they have proposed that either the magnitude of the *ab initio* imaginary frequency [ $379i \text{ cm}^{-1}$  at the CCSD/TZ(2df,2p) level]<sup>9(b)</sup> is four times too large, or the  $S_0/T_1$  interaction might play some role in the transition state region.

Very recently, the photodissociation of ketene on the triplet state has also been studied in the experimental work of Wodtke *et al.*<sup>10</sup> Metastable time-of-flight spectroscopy was used to measure the translational energy distribution of specific rotational state of CO formed from ketene photodissociation from  $T_1$  (351 nm–3.53 eV), which enables one to derive the correlated internal energy distribution of the other fragment,  $^3B_1 \text{ CH}_2$ . It has been found that the total  $\text{CH}_2$  rotational energy distribution cannot be reproduced by the impulsive model, and they have suggested that the internal rotation is coupled with the out-of-plane-bending motion in the transition state region and that better agreement might be obtained from an accurate theoretical calculation including the internal rotation as well as the out-of-plane-bending motion along the reaction coordinate.

Despite much attention and mystery about this reaction, there are only very limited theoretical works have been done on the photodissociation process. In addition to the early state correlation and *ab initio* studies by Yamabe and Morokuma,<sup>11</sup> the only available state-of-the-art calculations were done by Allen and Schaefer<sup>9</sup> and they have only considered the minimum and transition states on the  $T_1$  surface in two  $C_s$  symmetries. Other studies mainly concentrated on the vertical excitation energies and equilibrium properties.<sup>12</sup> Virtually no careful study has been carried out to characterize the nonadiabatic interaction in the photodissociation process.<sup>13</sup>

In the present paper, we have carried out *ab initio* studies on the low-lying electronic excited states of ketene. We feel that it is not likely that the vibrational frequency calcu-

<sup>a)</sup>Electronic mail: morokuma@emory.edu

lated at the CCSD/TZ(2d1f,2p) level is four times too large,<sup>7</sup> we shall pay particular attention to the nonadiabatic interaction between different electronic states.

## II. METHODS OF CALCULATION

Geometries of potential-energy minima and transition states are optimized using the analytical gradient at both the EOM-CCSD<sup>14</sup> and CASSCF level. In the CASSCF, the full valence active space excluding the two C–H bonds, (10e/9MO), consisting of 10 electrons in nine orbitals, is used with 6–31G(*d,p*), a valence double-zeta basis set with an associated polarization functions,<sup>15</sup> while a few points are also calculated with 6–311G(*d,p*).<sup>16</sup> Vibrational frequencies and zero-point energies (ZPEs) are calculated with the same method used for geometry optimization. Minima on the seam of crossing (MSX) are located also using the analytical gradient. Finally, single point calculations are performed at the CASPT2/PVTZ<sup>17</sup> level for better energetics, where PVTZ' is the Dunning correlation consistent triple-zeta basis set (PVTZ),<sup>18</sup> excluding *f* functions on C and O and *d* functions of H to save computational cost. Spin–orbit coupling matrix elements are also calculated at the singlet triplet crossing geometries, with an effective one-electron Hamiltonian approach.<sup>19</sup> The values shown below do not include the Franck–Condon factor.

ACES-II<sup>20</sup> was used for EOM-CCSD calculations, and the MOLPRO 96<sup>21</sup> was used for part of CASSCF and all CASPT2 calculations. The GAMESS<sup>22</sup> program was used to perform CASSCF optimization for transition states, vibrational analysis and spin–orbit coupling calculations. Our own program<sup>23,24</sup> in conjunction with HONDO 8.0 was employed for the MSX search.<sup>25</sup> The energies quoted in the text are at the CASPT2/PVTZ' level at the CASSCF/6–31G(*d,p*) optimized geometries, unless otherwise specified.

The symmetry and adiabatic dissociation limit of all the electronic states we consider in this work are summarized in Fig. 1 for reference. Geometries and energetics of important structures involved in the photodissociation are shown in Figs. 2 and 3 and Table I, respectively. In the discussion, we follow the definition of the two  $C_s$  symmetries:  $C_s$ -I for out of plane and  $C_s$ -II for in-plane C–C–O bend.<sup>9</sup>

## III. POTENTIAL-ENERGY SURFACES AROUND THE FRANCK–CONDON REGION: $S_0/S_1$ AND $S_1/T_n$ ( $n=1,2$ ) INTERACTIONS

In the Franck–Condon (F–C) region, the low-lying excited states are  $S_1(^1A_2)$ ,  $T_1(^3A_2)$ , and  $T_2(^3A_1)$  states. The second singlet excited state  $^1B_1$  is shown to be Rydberg in character<sup>12</sup> and is very high in the F–C region. Therefore, we do not include this in the discussion. The vertical excitation energy calculated at different levels of theory, in comparison with previous results, are shown in Table I. Generally, the agreements are good. It should be noted that the excitation from the ground state ( $^1A_1$ ) to the first singlet state ( $^1A_2$ ) is dipole forbidden, although it is the state that is accessed in most low-energy (~350 nm, 3.53 eV) experiments. Obviously, vibrational motions (at least zero-point motion) are

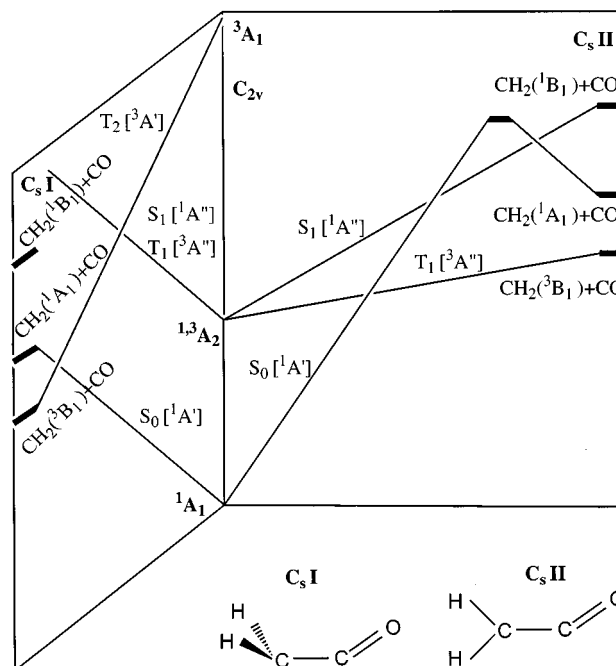


FIG. 1. State correlation diagram for the photodissociation of ketene in two  $C_s$  symmetries.

essential to the absorption process. We have calculated the transition dipole moments as a function of C–C–O bending angle in the two  $C_s$  symmetries. Although the magnitude of transition dipole moments does deviate from zero as one breaks the  $C_{2v}$  symmetry, the absolute value is still very small, in the order of  $10^{-2}$ – $10^{-1}$  a.u. No large difference was found between the two  $C_s$  symmetries.

The optimized structures we obtained are shown in Fig. 2. The minimum structures on  $S_0$ ,  $S_0$ – $C_{2v}$ , on  $S_1$ ,  $S_1$ – $C_s$ -II, and on the  $T_1$  and  $T_2$  are well known from earlier calculations,<sup>9,12</sup> and will not be discussed in detail. It is also known that  $S_1$  and  $T_1$  are strongly stabilized by C–C–O bending in  $C_s$ -II but not in  $C_s$ -I, while  $T_2$  is stabilized by C–C–O bending in  $C_s$ -I.<sup>11</sup> The minimum structure on  $T_1$ ,  $T_1$ – $C_s$ -II, has a structure similar to  $S_1$ – $C_s$ -II. The optimized structures of  $S_1$  and  $T_1$  under  $C_s$ -I symmetry constraint,  $S_1$ – $C_s$ -I and  $T_1$ – $C_s$ -I, are actually in  $C_{2v}$ , as shown in the Fig. 2. They are rather similar both in energy and in structure and lie 0.93 and 1.14 eV above the true  $S_1$  and  $T_1$  minima,  $S_1$ – $C_s$ -II and  $T_1$ – $C_s$ -II, respectively. Vibrational analysis indicates that these two  $C_s$ -I structures each have one imaginary frequency in  $a''$  irrep. (irreducible representation) and are the transition states for CO bend connecting  $S_1$ – $C_s$ -II and  $T_1$ – $C_s$ -II, respectively, and their equivalent isomers. The optimized structure for  $T_2$  under the  $C_s$ -I symmetry constraint,  $T_2$ – $C_s$ -I, is the transition state for  $CH_2$  rotation, connecting  $T_1$ – $C_s$ -II and its equivalent isomer. According to these results, it is expected that the molecule preferentially distorts to  $C_s$ -II symmetry after the absorption of the photon.

The issue, that we shall concentrate on is the nonadiabatic interactions between these low-lying states. We ask in the F–C region what modes are critical for the intersystem

TABLE I. Energies (in eV, relative to the ground-state equilibrium structure  $S_0-C_{2v}$ ) of various critical structures of ketene around the Franck–Condon region at various levels of theory at the (10e/9MO)-CASSCF optimized geometries. No zero-point energy corrections are added to the energies.

| Structure                 | CAS<br>I <sup>a</sup> | CASPT2<br>II <sup>a</sup> | EOM-<br>CCSD/I | EOM-<br>CCSD/II <sup>a</sup> | ZPE<br>(kcal/mol) <sup>a</sup> | Other works  |
|---------------------------|-----------------------|---------------------------|----------------|------------------------------|--------------------------------|--|
| $S_0(^1A_1)$              | 0.0                   | 0.0                       | 0.0            | 0.0                          | 20.0                           |  |
| $S_1(^1A_2)$ – <b>ver</b> |                       | 3.56                      | 3.92           | 3.98                         |                                | 3.97, <sup>b</sup> 3.84 <sup>c</sup> , 3.69 <sup>d</sup>   |
| $T_1(^3A_2)$ – <b>ver</b> |                       | 3.47                      | 3.79           | 3.84                         |                                | 3.83, <sup>b</sup> 3.79, <sup>c</sup><br>3.35 <sup>f</sup> |
| $T_2(^3A_1)$ – <b>ver</b> |                       | 5.27                      | 5.52           | 5.63                         |                                | 5.56, <sup>b</sup> 5.29, <sup>d</sup> 4.99 <sup>e</sup>    |
| $S_1-C_s$ - <b>I</b>      | 3.72                  | 3.37                      | 3.65           |                              | 18.3                           |  |
| $S_1-C_s$ - <b>II</b>     | 2.54                  | 2.44                      | 2.73           | 2.81                         | 20.1                           | 2.68 <sup>b</sup>  |
| $T_1-C_s$ - <b>I</b>      | 3.74                  | 3.31                      | 3.33           |                              | 18.4                           |  |
| $T_1-C_s$ - <b>II</b>     | 2.24                  | 2.17                      | 2.11           | 2.18                         | 19.8                           | 2.54, <sup>b</sup> 2.40 <sup>g</sup>                       |
| $T_2-C_s$ - <b>I</b>      | 2.60                  | 2.59                      | 2.51           | 2.58                         | 18.4                           |  |
| $S_0/S_1$ – <b>MSX</b>    | 2.76                  | 2.66                      |                |                              |                                |  |
| $S_0/S_1$ – <b>X</b> –1.4 | 3.17                  |                           |                |                              |                                |  |
| $S_0/S_1$ – <b>X</b> –1.7 | 3.13                  |                           |                |                              |                                |  |
| $S_1/T_1$ – <b>MSX</b>    | 3.77                  | 3.29                      |                |                              |                                |  |
| $S_1/T_2$ – <b>MSX</b>    | 3.89                  | 3.86                      |                |                              |                                |  |
| $T_1/T_2$ – <b>MSX</b>    | 3.92                  | 3.88                      |                |                              |                                |  |

<sup>a</sup>CAS is (10e/9MO)-CASSCF and CASPT2 is (10e/9MO)-CASPT2. Basis set I is 6-31G(*d,p*); basis II is PVTZ', the Dunning correlation consistent PVTZ basis set excluding *f* functions on C and O and *d* functions on H; and basis III is 6-311G(*d,p*). ZPE is the zero-point energy (in kcal/mol) at the CAS/I level.

<sup>b</sup>From the EOM-CCSD/PBS calculation in Ref. 12.

<sup>c</sup>Reference 6 in Ref. 12.

<sup>d</sup>From electron impact energy-loss spectra, Ref. 8 in Ref. 12.

<sup>e</sup>From Ref. 9 in Ref. 12.

<sup>f</sup>From Ref. 4 in Ref. 12.

<sup>g</sup>From Ref. 9.

crossing ( $S_1/T_n$ ) and the internal conversion ( $S_1/S_0$ ) process. Therefore, we have located the minima on the seam of the crossing between these states in the two  $C_s$  symmetries. The structures thus obtained are shown in Fig. 2.

First of all, we found that the lowest point where  $S_0$  and  $S_1$  crossed was the structure  $S_0/S_1$ –**MSX** in the  $C_s$ -II symmetry. Compared with the minimum on  $S_1$ ,  $S_1$ – $C_s$ -**II**, the C–C–O angle is further compressed from 128.3° to 115.8°, and C–C is stretched from 1.455 to 1.528 Å. Since the energy of the  $S_0/S_1$ –**MSX** is only 2.66 eV, lower than the typical photon energy of 3.53 eV (350 nm) used in the experiments, we have also looked for crossing structures between  $S_0$  and  $S_1$  at higher energy. We restricted the C–C distance to 1.40 and 1.70 Å in the MSX search, on both sides of the real  $S_0/S_1$ –**MSX**, to find the structures  $S_0/S_1$ –**X**–1.4, and  $S_0/S_1$ –**X**–1.7, respectively, in Fig. 2. It is seen that only the C–C–O angle changes significantly as one varies the C–C distance on the seam of the crossing. Table I shows that the energies of the two structures are 0.41 and 0.37 eV, respectively, higher than that of  $S_0/S_1$ –**MSX** at the CASSCF level, still below the photon energy. The seam of the crossing, passing through  $S_0/S_1$ –**X**–1.4,  $S_0/S_1$ –**MSX**, and  $S_0/S_1$ –**X**–1.7, lies in the vicinity of the  $S_1$  minimum,  $S_1$ – $C_s$ -**II**. A trajectory starting from the F–C geometry on the  $S_1$  potential surface and traveling down to the  $S_1$  minimum will have many chances to cross the seam, and therefore, the internal conversion process is expected to be very efficient and immediate after the absorption of the photon. In fact, no fluorescence has been observed experimentally in the photolysis of ketene.<sup>12</sup> Since  $S_0$  and  $S_1$  belong to  $A'$  and  $A''$  irrep., respectively, in  $C_s$ -II symmetry, the

$A''$  H–C–O out-of-plane torsion couples these two states and is an critical mode for the internal conversion. It should be mentioned that a partially optimized  $S_0/S_1$  crossing structure was also found in the earlier work of Yoshimine.<sup>13</sup> Finally, since the lowest structure of  $S_1$  is rather high in  $C_s$ -I, it is not expected to cross with  $S_0$  at low energy. Therefore, no attempt was made to search for MSX between  $S_0$  and  $S_1$  in  $C_s$ -I.

We have also studied the intersection between  $S_1$  and  $T_n$  ( $n=1,2$ ) states in the F–C region. It is found that the  $S_1$  and  $T_1$  states are very close in energy in the F–C region. The optimization of the MSX structure under the  $C_s$ -I constraint actually converged the  $C_{2v}$  structure  $S_1/T_1$ –**MSX**, with a low energy of 3.29 eV, as shown in Fig. 2. It is seen that the C–C distance is quite short, 1.390 Å, compared to  $\sim 1.45$  Å in the  $S_1$  and  $T_1$  equilibrium structures. The spin–orbit coupling element  $\langle H^{SO} \rangle$  between the two states should be zero, because they both belong to the  $A_2$  irrep. in the  $C_{2v}$  symmetry and, therefore, no  $l$  component contributes to the spin–orbit coupling matrix element. Actual calculations in the  $C_s$  constraint gives a negligible  $\langle H^{SO} \rangle$ . As C–C–O bends,  $l_z s_z$  starts to contribute to  $\langle H^{SO} \rangle$ ; however, both states have similar electronic configurations ( $\pi_{\perp n}(C-C-O) \rightarrow \pi_{\parallel}^*(C-O)$ ), which implies that the norm of the coupling will be small. For example, it is well known that the spin–orbit coupling between the  $\pi$ – $\pi^*$   $S/T$  states is small, while that between  $\pi$ – $\pi^*$  and  $n$ – $\pi^*$  states is much larger.<sup>26</sup> Therefore, we conclude that the direct intersystem crossing from  $S_1$  to  $T_1$  is not efficient.

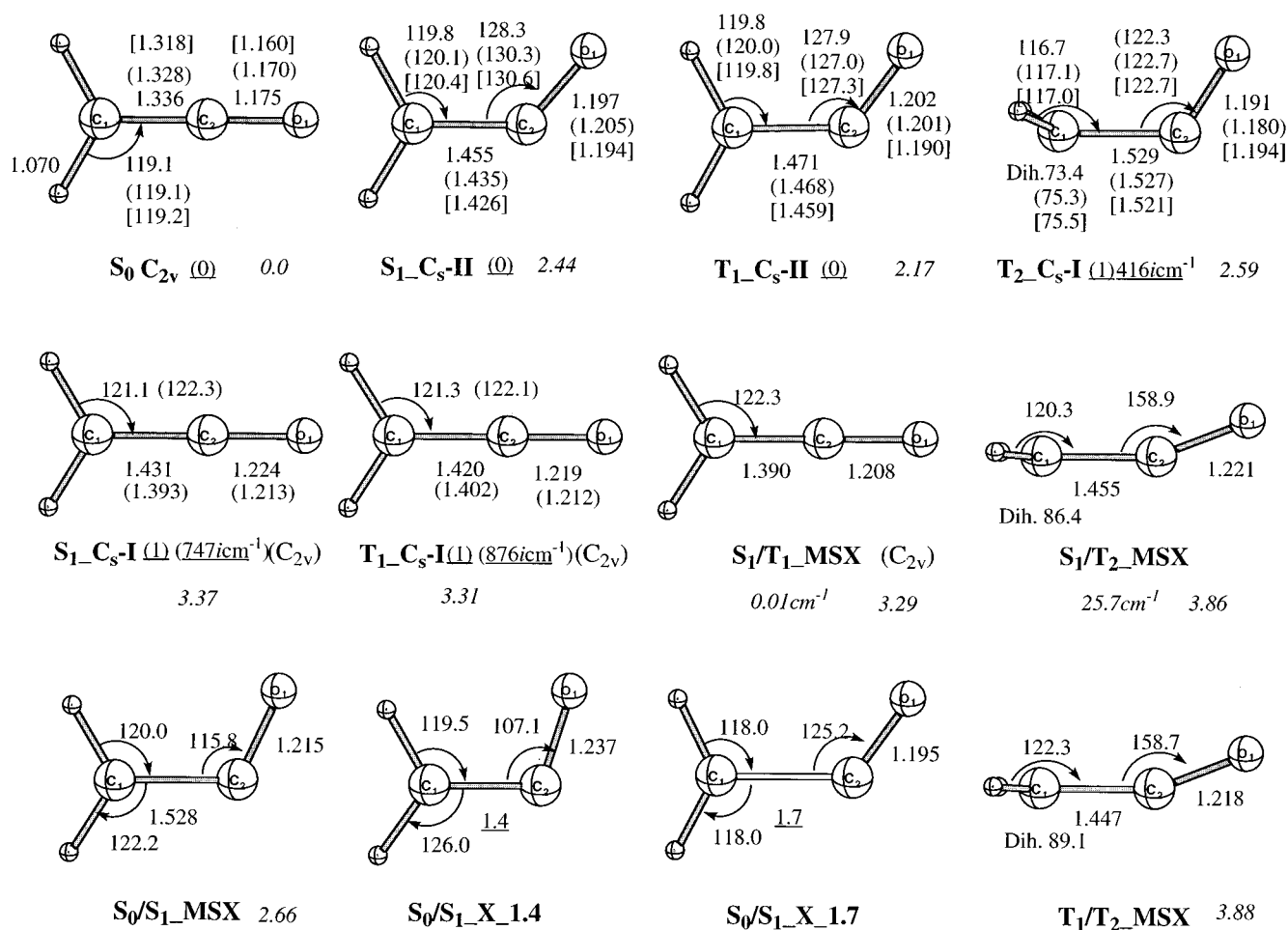


FIG. 2. Optimized structures (in Å and degree) of ketene around the F-C region. On the structures, plain numbers are obtained at the (10e/9MO)-CASSCF/I level, numbers in parentheses at the EOM-CCSD/I level, and numbers in brackets at the EOM-CCSD/I level (using CCSD for EOM-CCSD for the  $S_0$  state). The underlined numbers are frozen. Beside the structural symbols are the (10e/9MO)-CASPT2/II energy (in eV, relative to the  $S_0\text{-}C_{2v}$ , in italic), and the (10e/9MO)-CASSCF/I spin-orbit coupling element (in  $\text{cm}^{-1}$ , in italic), as well as the number (in parentheses, underlined) and values (in  $\text{cm}^{-1}$ , underlined) of CASSCF/I imaginary frequencies.

We have found that  $S_1$  and  $T_1$  cross with  $T_2$  in  $C_s\text{-I}$  symmetry at the structures  $S_1/T_2\text{-MSX}$  and  $T_1/T_2\text{-MSX}$ , respectively, as shown in the Fig. 2. The two structures are very similar, and the C-C-O angle is  $\sim 159^\circ$ , nearly linear. In fact, the  $S_1\text{-}T_2$  and  $T_1\text{-}T_2$  crossings are not surprising. As shown in Fig. 1, in the  $C_s\text{-I}$  symmetry,  $S_1$  and  $T_1$  correlate adiabatically to the higher excited states of the dissociation product of  $\text{CH}_2+\text{CO}$ , while  $T_2$  correlates to the ground state of  $\text{CH}_2+\text{CO}$ . Since  $T_2$  is higher in energy than  $S_1$  and  $T_1$  at the F-C geometry, they must undergo crossing somewhere. Our results show clearly that this happens very near the F-C region, where the C-C distance is only  $\sim 1.45$  Å, and the C-C-O angle is  $\sim 160.0^\circ$ . The energies of these two structures, 3.86 and 3.88 eV, are higher than the typical experimental photon energy of 3.52 eV (350 nm). The norm of the spin-orbit coupling element between  $S_1$  and  $T_2$  is  $25.7\ \text{cm}^{-1}$  at  $S_1/T_2\text{-MSX}$ , and are much larger than that between  $S_1$  and  $T_1$  at  $S_1/T_1\text{-MSX}$ . As we have discussed earlier, this is due to that fact that  $S_1$  and  $T_2$  have different electronic configurations [ $\pi_{\perp n}(\text{C-C-O})\rightarrow\pi_{\perp}^*(\text{C-C-O})$  for

$T_2$ ]. Due to the high energy of the crossing structure  $S_1/T_2\text{-MSX}$ , the intersystem crossing from  $S_1$  to  $T_2$  is not likely to contribute to the photodissociation process, except for photodissociation at a shorter wavelength where it may compete with the  $S_1\text{-}S_0$  internal conversion. No low-energy crossing between  $S_1$  or  $T_1$  and  $T_2$  is found in  $C_s\text{-II}$ , which is not surprising because in  $C_s\text{-II}$ ,  $S_1$  and  $T_1$  correlate to the low-lying states of products, and  $T_2$  correlates to the high excited states.

As a short summary, according to the above calculations, we have seen that after the absorption of a photon of 350 nm (3.53 eV) range, the molecule will preferentially fall into the  $C_s\text{-II}$  symmetry, where the possibility of direct crossing from  $S_1$  to  $T_1$  is very small due to the vanishingly small spin-orbit coupling element. Rather, the molecule is likely to undergo with a very high probability an internal conversion to the  $S_0$  state. The hot molecule in  $S_0$  then may dissociate adiabatically into the excited products in singlet, if there is enough energy for the adiabatic dissociation. If there is not enough energy, it has to cross over to the  $T_1$  or  $T_2$  state and

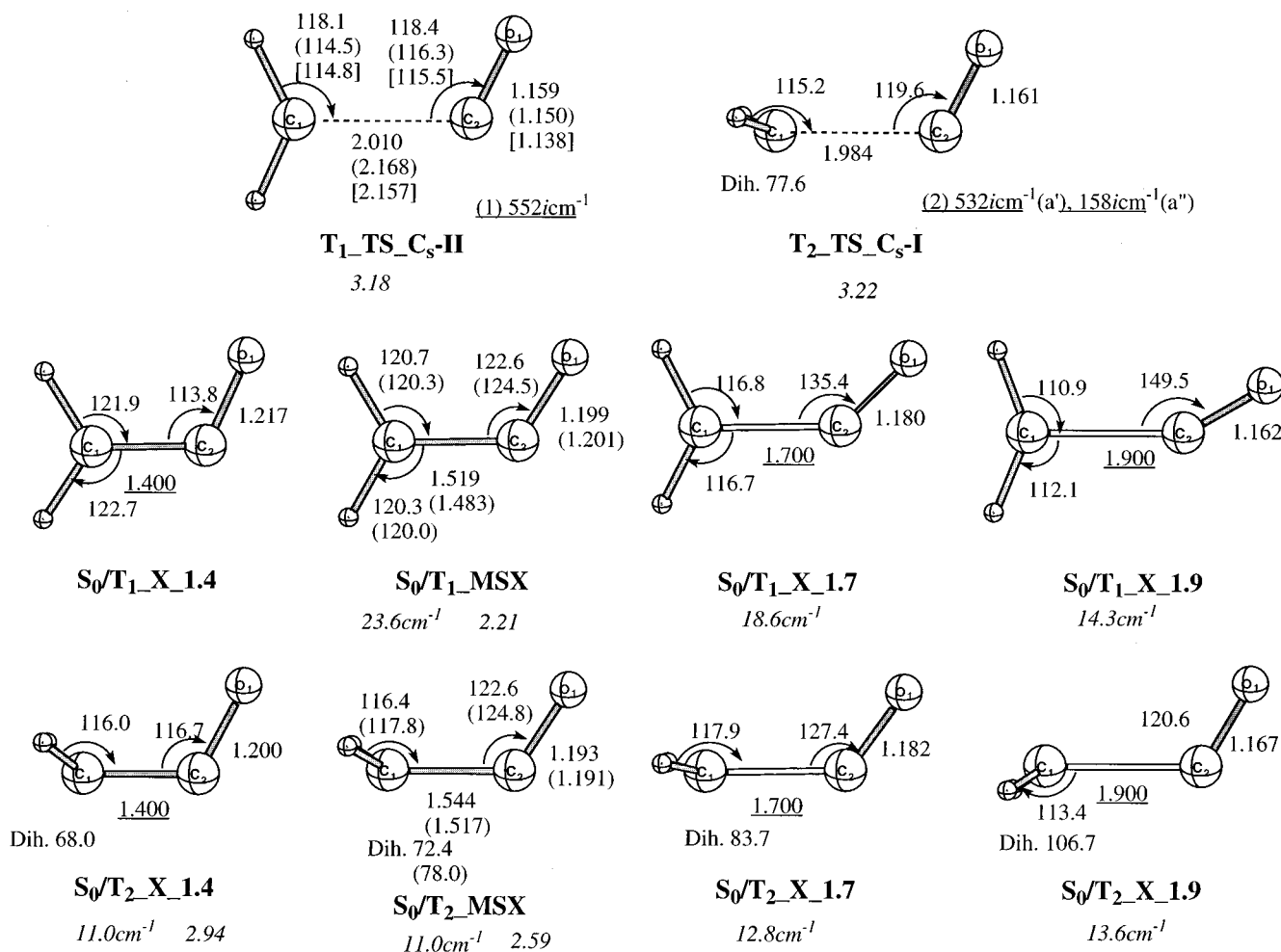


FIG. 3. Optimized structures (in Å and degree) of ketene molecule along the dissociation pathway. For notations, see Fig. 2.

dissociates into the ground-state products in triplet. Experimentally, it has been found that the singlet/triplet product branching ratio increases from 0 to 2 in the first 125 cm<sup>-1</sup> above the singlet threshold.<sup>27</sup> At a higher excess energy of 2365 cm<sup>-1</sup> above the singlet threshold, no triplet products were observed in either the molecular beam study of Hayden *et al.*<sup>28</sup> or the vacuum UV induced fluorescence study of Nesbitt *et al.*<sup>29</sup>

#### IV. POTENTIAL-ENERGY SURFACES ALONG THE DISSOCIATION REACTION COORDINATES: S<sub>0</sub>/T<sub>n</sub> (n=1,2) INTERACTION

In this section, we consider the interaction between the T<sub>n</sub> (n=1,2) states and the S<sub>0</sub> state along the dissociation reaction coordinate, because they are the states correlate to the two lowest asymptotic of CH<sub>2</sub>+CO. As clearly shown in the earlier studies,<sup>11,9</sup> S<sub>0</sub> dissociation to (<sup>1</sup>A<sub>1</sub>) CH<sub>2</sub>+CO is orbital forbidden in C<sub>s</sub>-II, but allowed and barrierless in C<sub>s</sub>-I. As also indicated in the Fig. 1, T<sub>1</sub> dissociates to the ground state (<sup>3</sup>B<sub>1</sub>) CH<sub>2</sub>+CO in C<sub>s</sub>-II, while in C<sub>s</sub>-I symmetry, T<sub>2</sub> does so. The dissociation transition state on T<sub>1</sub>, T<sub>1</sub>-TS-C<sub>s</sub>-II, and the second-order saddle point on T<sub>2</sub>, T<sub>2</sub>-TS-C<sub>s</sub>-I, with an imaginary frequency for dissociation

(a') and another for CH<sub>2</sub> rotation (a''), with the optimized structures shown in Fig. 3, are well characterized.<sup>9,7</sup> Therefore, we will not discuss them in detail, but note two points. The imaginary vibrational frequencies at T<sub>1</sub>-TS-C<sub>s</sub>-II, 552i and 403i cm<sup>-1</sup> at the CASSCF/I and CCSD/I level, respectively, are not far from Allen and Schaefer's 379i cm<sup>-1</sup>.<sup>9(b)</sup> At the CASPT2/II level, the energy of T<sub>1</sub>-TS-C<sub>s</sub>-II is lower than the dissociation limit without the ZPE and becomes higher only with ZPE; this may be due to the fact that the CASSCF optimized transition state is a little too early.

What we found interesting was the crossing structures between the S<sub>0</sub> and T<sub>n</sub> (n=1,2) states. In C<sub>s</sub>-II, we have located between S<sub>0</sub> and T<sub>1</sub> the MSX structure S<sub>0</sub>/T<sub>1</sub>-MSX and also some restricted MSX structures with the C-C distance fixed at 1.40, 1.70, and 1.90 Å, respectively. We have obtained in the C<sub>s</sub>-I symmetry the MSX structure S<sub>0</sub>/T<sub>2</sub>-MSX and some restricted MSX structures between S<sub>0</sub> and T<sub>2</sub>. The obtained structures are shown in Fig. 3 with quite obvious notations.

In C<sub>s</sub>-II, S<sub>0</sub>/T<sub>1</sub>-MSX is very close in geometry to the T<sub>1</sub> equilibrium structure T<sub>1</sub>-C<sub>s</sub>-II. This would imply that the T<sub>1</sub> molecule will be produced at this crossing mainly in

TABLE II. Energies (in eV, relative to the ground-state equilibrium structure  $S_0-C_{2v}$ ) of various critical structures of ketene along the dissociation pathway at various levels of theory at the (10e/9MO)-CASSCF optimized geometries. No zero-point energy is added to the energies. Definition of the basis sets and methods is the same as in Table I.

| Structure        | CAS/I | CASPT2/II | CCSD/I | CCSD/II' | ZPE<br>(kcal/mol) | Reverse barrier<br>height <sup>a</sup> |
|------------------|-------|-----------|--------|----------|-------------------|--|
| $T_1-TS(^3A'')$  | 2.95  | 3.18      | 3.23   | 3.28     | 16.6              | 0.17                                   |
| $T_2-TS(^3A')$   | 3.02  | 3.22      |        |          | 16.5              | 0.41                                   |
| $S_0/T_1-X-1.4$  | 2.60  |           |        |          |                   |  |
| $S_0/T_1-MSX$    | 2.31  | 2.21      | 2.12   |          |                   |  |
| $S_0/T_1-X-1.7$  | 2.72  |           |        |          |                   |  |
| $S_0/T_1-X-1.9$  | 3.51  |           |        |          |                   |  |
| $S_0/T_2-X-1.4$  | 2.94  |           |        |          |                   |  |
| $S_0/T_2-MSX$    | 2.62  | 2.59      | 2.51   |          |                   |  |
| $S_0/T_2-X-1.7$  | 2.82  |           |        |          |                   |  |
| $S_0/T_2-X-1.9$  | 3.11  |           |        |          |                   |  |
| $CO+CH_2(^3B_1)$ | 2.31  | 3.24      | 2.99   | 3.01     | 14.1              | 0.00                                   |

<sup>a</sup>From Ref. 9.

the vibrational ground state because of the Franck–Condon factor. In the restricted MSX structures, only the H–C–C angles and the O–C–C angle change significantly from that of  $S_0/T_1-MSX$ . Near the F–C structure with the C–C distance fixed at 1.40 Å, the O–C–C angle is compressed from 122.6° in  $S_0-T_1-MSX$  to ~113.8°. For  $S_0/T_1-X-1.7$  and  $S_0/T_1-X-1.9$ , both O–C–C and H–C–H angles open up and deviate substantially from the minimum energy dissociation path. For instance, in  $S_0/T_1-X-1.9$ , the O–C–C angle is 149.5°, far from ~116.3° in the dissociation transition state. The energies of these crossing structures are lower than the typical experimental photon energy of 3.52 eV, as seen in Table II. In the  $C_s$ -II symmetry,  $S_0$  is  $^1A'$  and  $T_1$  is  $^3A''$ , therefore, both  $l_x s_x$  and  $l_y s_y$  contributes to  $\langle H^{SO} \rangle$ . The norm of calculated spin–orbit coupling element  $\langle H^{SO} \rangle$  between  $S_0$  and  $T_1$  at these structures, also shown in Fig. 3, is quite large, suggesting a strong coupling. The norm decreases somewhat as the C–C distance increases. As discussed above,  $S_1$  does not couple with  $T_1$  strongly in  $C_s$ -II and the direct  $S_1 \rightarrow T_1$  intersystem crossing is unlikely. However, the coupling  $S_0$  to  $T_1$  is quite strong, as is the  $S_1-S_0$  coupling. Therefore, the dissociation pathway of ketene at low photon energy is most likely to be:  $S_1 \rightarrow S_0 \rightarrow T_1 \rightarrow CH_2(^3B_1) + CO$ .

We also find an interesting singlet–triplet crossing in  $C_s$ -I. The MSX between  $S_0$  and  $T_2$ ,  $S_0/T_2-MSX$ , is also very similar to the structure  $T_2-C_s-I$ , on the  $T_2$  surface, which is a transition state for  $CH_2$  rotation. As one freezes the C–C distance, there is a small variation of the O–C–C angle in the restricted MSX structures. However, the H–C–C–O dihedral angle changes more significantly. At the  $S_0/T_2-MSX$ , the H–C–C–O dihedral angle is 72.4°, at  $S_0/T_2-X-1.7$  it becomes 83.7°, and more interestingly, at  $S_0/T_2-X-1.9$ , it becomes 106.7°, larger than 90°. Compared to the dissociation “TS” within  $C_s$ -I,  $T_2-TS-C_s-I$ , the C–C distance and the O–C–C angle are similar, yet the  $CH_2$  fragment is inverted. The energy of these restricted MSX structures are all lower than the photon energy of ~3.52 eV. Comparing the energies of  $S_0/T_2-X-R$  in  $C_s$ -I with those of  $S_0/T_1-X-R$  in  $C_s$ -II, as shown in Table II,

the restricted MSXs for short C–C distances,  $S_0/T_2$  crossings are higher in energy than  $S_0/T_1$  crossings. While for longer C–C distances,  $S_0/T_2$  crossings becomes lower in energy. For instance,  $S_0/T_2-X-1.9$  is considerably lower than  $S_0/T_1-X-1.9$ . It might be related to the fact that  $S_0$  dissociation is orbital forbidden in  $C_s$ -II, and therefore, lies higher in energy than in  $C_s$ -I for considerably stretched C–C distances. In  $C_s$ -I, both states ( $S_0$  and  $T_1$ ) belong to the  $A'$  irrep., and therefore, only  $l_z s_z$  contributes to  $H^{SO}$  and the coupling matrix element is pure imaginary. In Fig. 3, only its absolute value is shown. In contrast to the case of  $C_s$ -II, the magnitude of spin–orbit coupling element increases slightly as C–C is stretched, and is smaller than that between  $S_0$  and  $T_1$  in  $C_s$ -II.

Although we have restricted our potential-energy search to  $C_s$ -II and  $C_s$ -I symmetries (see Fig. 4), one should note that the  $T_1$  state in the  $C_s$ -II symmetry connects smoothly to the  $T_2$  state in the  $C_s$ -I symmetry via  $C_1$  symmetry. This means the transition state  $T_1-TS-C_s-II$  at 3.18 eV is connected smoothly to the second-order transition state  $T_2-TS-C_s-I$  at 3.22 eV. Although we have not examined the structures in the  $C_1$  symmetry, one would expect that a relatively flat ridge of the “transition state” between ketene and the dissociation products should persist all along the internal rotation of the  $CH_2$  group from  $C_s$ -II to  $C_s$ -I. The situation would be also similar for the seam of the crossing. Upon the  $CH_2$  internal rotation, the minimum seam of the crossing, starting with  $S_0/T_1-MSX$  in  $C_s$ -II, should persist in the  $C_1$  symmetry and connect smoothly to  $S_0/T_2-MSX$  in  $C_s$ -I. Thus, the dynamic processes we have been discussing only in  $C_s$ -II and  $C_s$ -I should apply at least qualitatively to all the geometries in the  $C_1$  symmetry, and the reaction can occur at any symmetry.

It is interesting to briefly consider the competition between the intersystem crossing and internal conversion from the  $S_1$  state. For a qualitative estimation of the transition probability, the simple Landau–Zener (LZ)<sup>30</sup> formula can be used. According to LZ, the probability of hopping from one adiabatic state to the other is, in general, given by

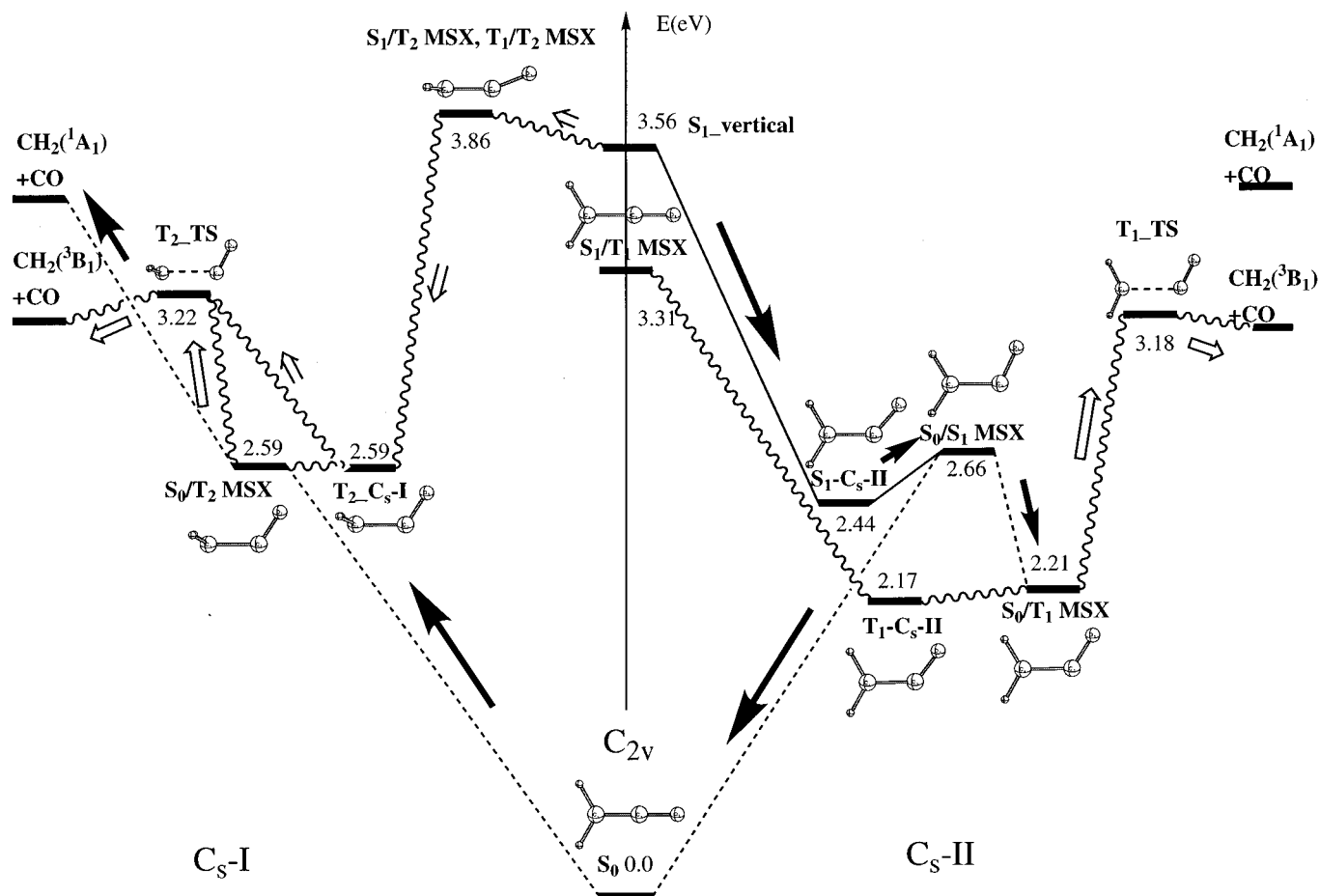


FIG. 4. The potential-energy profiles for photodissociation in  $C_s$ -I and  $C_s$ -II symmetries. The labels of the structures coincide with those in Figs. 2 and 3. The solid arrows are for probable pathways on singlet potential surfaces, and open arrows are for those on triplet potential surfaces.

$P = \exp[-(\pi/4)\xi]$ , where  $\xi$  is the Massey parameter. The transition between states with different spin multiplets can be handled most conveniently in the diabatic representation, and the Massey parameter is given  $\xi = 8(H_{S_0})^2/(\hbar\Delta F v_{\parallel})$ , where  $\Delta F$  is the difference in the energy slope between the two states and  $v_{\parallel}$  is the velocity of the nuclei in the direction tangent to the crossing seam. The transition between two adiabatic states caused by the derivative coupling matrix element can be handled conveniently in the adiabatic representation,<sup>31,32</sup> and the Massey parameter is given by  $\xi = \Delta E/(\hbar v_{\perp} d)$ , where  $d$  is the derivative coupling matrix element between the two adiabatic electronic states and  $v_{\perp}$  is the velocity of the nuclei along the direction of the derivative coupling. At the  $S_0/S_1$ -MSX, we have computed analytically the derivative coupling element between the  $S_0(1A')$  and  $S_1(1A'')$  states with the CASSCF wave function.<sup>33</sup> The magnitude of the nonadiabatic coupling element  $d$ , thus calculated, is  $\sim 30 \text{ bohr}^{-1}$ . The velocity  $v_{\perp}$  should be that in the symmetry breaking modes, because  $S_0$  and  $S_1$  belong to different spatial symmetry. Using the normal mode of one  $a''$  H-C-C-H torsion mode ( $1061 \text{ cm}^{-1}$ ) at the  $S_1$  minimum, we have estimated the velocity along the symmetry breaking direction and then obtained the Massey parameter  $\ll 1$ , which indicates that the internal conversion from  $S_1$  to  $S_0$  is ex-

pected to be very efficient. The intersystem crossing probability is harder to estimate. Using  $H^{S_0} \sim 20 \text{ cm}^{-1}$  (from Fig. 3),  $v_{\parallel} \sim 10^3 \text{ m/s}$  (the order of magnitude velocity of the C-C-O bending ground state) and  $\Delta F \sim 0.01 \text{ hartree/bohr}$ , one obtains the transition probability of  $\sim 0.01$ . Clearly, the internal conversion is much more favored over the intersystem crossing.

The exact effect of the intersystem crossing between the  $S_0$  and  $T_n$  ( $n=1,2$ ) states on the microcanonical rate constant of the triplet ketene is not very clear at the moment. On one hand, we have found that the MSX between the  $S_0$  and  $T_n$  ( $n=1,2$ ) states are energetically well below the triplet dissociation transition states. Therefore, one tends to think that the intersystem crossing is relatively fast compared to the dissociation process as the total energy is quite high. As a result, the dissociation on the triplet state can just be described with the standard statistical model on a single potential surface. However, this certainly cannot explain the sharp stair structure in the rate constant found in Moore's experiment or why tunneling does not destroy the stair structure as found in the theoretical study of Miller *et al.* Since the MSX lies very close to the minimum on the triplet states, the trajectory has a large possibility of recrossing back and forth between the  $S_0/T_n$  states, even though the spin-orbit cou-

pling is not exceedingly large. A similar situation has been analyzed by Miller and co-workers in the study of the quenching process of  $O(^1D)$  by  $N_2$ .<sup>34</sup>

On the other hand, we have shown that  $S_0$  and  $T_n$  cross *all along* the dissociation path. In contrast, if the molecule undergoes a nonadiabatic transition at a crossing, which is high in energy, in particular, close in energy to that of the transition state on the triplet state, the corresponding trajectory has a large probability to dissociate. Therefore, the crossings at higher energies might play an important role in the overall dissociation process. In addition, we have found that the crossing structures at higher energies generally deviate substantially from the minimum energy path on the triplet states. The energy gradient vector<sup>35</sup> at  $S_0/T_1$ -**MSX** represents mainly the O-C-C bending motion. This O-C-C bending is also the promotion mode for direct passage from the high-energy  $S_0/T_1$  crossing structure to  $T_1$ -**TS-C<sub>s</sub>-II**, as can be seen in the  $S_0/T_1$ -**X-1.9**. This means that the promotion mode is different from the reaction path motion, which reduces the effect of the tunneling process, thus, prevents the stair structure in the rate constant from being washed out. At  $S_0/T_2$ -**MSX** the energy gradient vector consists of the O-C-C bending and the CH<sub>2</sub> wagging. These modes are promotion modes for direct passage from the high-energy  $S_0/T_2$  crossing structure to  $T_2$ -**TS-C<sub>s</sub>-I**, as can be seen in the  $S_0/T_2$ -**X-1.9**. Again, the promotion modes are different from the reaction path motion. The CH<sub>2</sub> wagging in the process may cause the CH<sub>2</sub> product rotation along the *a* axis, as has been observed by Wodtke *et al.*<sup>10</sup>

Obviously, much more quantitative work based on quantum dynamics has to be done to further clarify the role of these  $S_0/T_n$  crossings. Currently, we are planning to carry out a two-dimensional model quantum calculation to examine the relative importance of the crossings at lower and higher energy.

## V. CONCLUSIONS

We have carried out *ab initio* calculations on the photodissociation of ketene, paying particular attention to the nonadiabatic interactions between the low-lying electronic states. We can summarize our findings as the following:

- (1)  $S_0$  and  $S_1$  states cross extensively around the F-C region in the  $C_s$ -II symmetry. The promoting modes are the C-C-O bending, which brings the two states close, and the H-C-C-O out-of-plane torsion, which couples the two states of different symmetry. A trajectory on  $S_1$  from the F-C geometry can cross  $S_0$  many times, as it travels down the  $S_1$  potential surface in  $C_s$ -II to the  $S_1$ -**C<sub>s</sub>-II** minimum and the  $S_1/S_0$ -**MSX**. Therefore, the  $S_1 \rightarrow S_0$  internal conversion is expected to be very efficient.
- (2)  $S_1$  and  $T_1$  stay close in energy in the F-C region. However, they do not couple strongly due to the vanishingly small spin-orbit coupling element. Therefore, the direct  $S_1 \rightarrow T_1$  intersystem crossing is weak. The triplet state molecule, which produces the ground-state products is likely to be formed via the process  $S_1 \rightarrow S_0 \rightarrow T_n$ .
- (3)  $S_0$  crosses with  $T_1$  in the  $C_s$ -II symmetry and  $T_2$  in the  $C_s$ -I symmetry all along the dissociation pathway. As C-C is stretched further out, the energy of the crossing increases and the crossing structure deviates substantially from the reaction path, although the norm of the spin-orbit coupling does not change significantly. The effect of the intersystem crossing on the dissociation rate constant depends on the relative importance of the crossings at lower and higher energies. If the former is the most important, the dissociation process should be described well with a statistical theory on a single potential-energy surface. On the other hand, if the crossings at higher energy play more important roles, the dynamics of the intersystem crossing process and the following dynamics on the triplet surface are expected to control the rate. The expected effect of this would be to reduce the tunneling, therefore, prevent the stair structure in the rate constant from being washed out. A quantum dynamics study is underway to further clarify the relative importance of the crossings at different energies.
- (4) At a higher photon energy ( $>3.9$  eV),  $S_1$  strongly couples with  $T_2$  in  $C_s$ -I, and the direct  $S_1 \rightarrow T_2$  intersystem crossing, followed by dissociation on the  $T_2$  potential surface in  $C_s$ -I, may become an important triplet pathway.

## ACKNOWLEDGMENTS

The authors would like to acknowledge Dr. S. J. Klippenstein, Dr. C. B. Moore, Dr. J. M. Bowman, and Dr. W. H. Miller for discussions. The authors are also grateful to Dr. John Stanton for making the ACESII program available and for discussion. One of the authors (Q.C.) acknowledges a graduate fellowship from the Phillips Petroleum Co. This work was in part supported by Grant No. F49620-95-1-0182 from the Air Force Office of Scientific Research.

<sup>1</sup>E. R. Lovejoy and C. B. Moore, *J. Chem. Phys.* **98**, 7846 (1994); E. R. Lovejoy, S. K. Kim, R. A. Alvarez, and C. B. Moore, *ibid.* **95**, 4081 (1991).

<sup>2</sup>J. D. Gezelter and W. H. Miller, *J. Chem. Phys.* **103**, 7868 (1995).

<sup>3</sup>I. Garcia-Moreno, E. R. Lovejoy, and C. B. Moore, *J. Chem. Phys.* **100**, 8890, 8902 (1994); W. H. Green, A. J. Mahoney, Q. K. Zheng, and C. B. Moore, *ibid.* **94**, 1961 (1991).

<sup>4</sup>C. G. Morgan, M. Drabbels, and A. M. Wodtke, *J. Chem. Phys.* **104**, 7460 (1996).

<sup>5</sup>S. J. Klippenstein and R. A. Marcus, *J. Chem. Phys.* **93**, 2481 (1990); S. J. Klippenstein, A. L. L. East, and W. D. Allen, *ibid.* **105**, 118 (1996).

<sup>6</sup>S. K. Kim, E. R. Lovejoy, and C. B. Moore, *J. Chem. Phys.* **102**, 3202 (1995).

<sup>7</sup>J. D. Gezelter and W. H. Miller, *J. Chem. Phys.* **104**, 3553 (1996).

<sup>8</sup>T. Seideman and W. H. Miller, *J. Chem. Phys.* **97**, 2499 (1992).

<sup>9</sup>(a) W. D. Allen and H. F. Schaefer III, *J. Chem. Phys.* **89**, 329 (1988); (b) (unpublished), as cited in Ref. 7.

<sup>10</sup>C. G. Morgan, M. Drabbels, and A. M. Wodtke, *J. Chem. Phys.* **105**, 4550 (1996).

<sup>11</sup>S. Yamabe and K. Morokuma, *J. Am. Chem. Soc.* **100**, 7551 (1978).

<sup>12</sup>P. G. Szalay, A. G. Csaszar, and L. Nemes, *J. Chem. Phys.* **105**, 1034 (1996), and references therein.

<sup>13</sup>M. Yoshimine, *J. Chem. Phys.* **90**, 378 (1989).

<sup>14</sup>See, for example, J. F. Stanton and R. J. Bartlett, *J. Chem. Phys.* **98**, 7029 (1993).

<sup>15</sup>P. C. Hariharan and J. A. Pople, *Mol. Phys.* **27**, 209 (1971), and references therein.

- <sup>16</sup>R. Krishnan, J. S. Binkley, R. Seeger, and J. A. Pople, *J. Chem. Phys.* **72**, 650 (1980).
- <sup>17</sup>See, for example, K. Anderson and B. Roos, in *Modern Electronic Structure Theory*, edited by D. Yarkony (World Scientific, Singapore, 1995).
- <sup>18</sup>T. H. Dunning, *J. Chem. Phys.* **90**, 1007 (1989).
- <sup>19</sup>S. Koseki, M. W. Schmidt, and M. S. Gordon, *J. Phys. Chem.* **96**, 10 768 (1992).
- <sup>20</sup>ACESII, J. F. Stanton, J. Gauss, W. J. Lauderdale, J. D. Watts, and R. J. Bartlett.
- <sup>21</sup>MOLPRO96, P. J. Knowles and H.-J. Werner.
- <sup>22</sup>GAMESS, M. W. Schmidt, K. K. Baldrige, J. A. Boatz, S. T. Elbert, M. S. Gordon, J. H. Jensen, S. Koseki, N. Matsunaga, K. A. Nguyen, S. J. Su, T. L. Windus, M. Dupuis, and J. S. Montgomery, *J. Comp. Chem.* **14**, 1347 (1993).
- <sup>23</sup>Q. Cui and K. Morokuma (unpublished).
- <sup>24</sup>K. M. Dunn and K. Morokuma, *J. Chem. Phys.* **102**, 4904 (1995).
- <sup>25</sup>N. Koga and K. Morokuma, *Chem. Phys. Lett.* **119**, 371 (1985).
- <sup>26</sup>N. J. Turro, *Modern Molecular Photochemistry* (University Science Books, Mill Valley, CA 1991).
- <sup>27</sup>I.-C. Chen, W. H. Green, Jr., and C. B. Moore, *J. Chem. Phys.* **89**, 314 (1988).
- <sup>28</sup>C. C. Hayden, D. M. Neumark, K. Shobatake, R. Sparkes, and Y. T. Lee, *J. Chem. Phys.* **76**, 3607 (1982).
- <sup>29</sup>D. J. Nesbitt, H. Petek, M. F. Foltz, S. V. Filseth, D. J. Bamford, and C. B. Moore, *J. Chem. Phys.* **93**, 223 (1985).
- <sup>30</sup>See, for example, M. S. Child, *Molecular Collision Theory* (Academic, London, 1974).
- <sup>31</sup>See, for example, H. Nakamura, in *Dynamics of Molecules and Chemical Reactions*, edited by R. E. Wyatt and J. Z. H. Zhang (Dekker, New York, 1996).
- <sup>32</sup>M. Desouter-Lecomte and J. C. Lorquet, *J. Chem. Phys.* **71**, 4391 (1979).
- <sup>33</sup>In MOLPRO, we forced a  $C_1$  symmetry by distorting the H-C-C-H dihedral angle by  $0.001^\circ$ .
- <sup>34</sup>G. E. Zahr, R. K. Preston, and W. H. Miller, *J. Chem. Phys.* **62**, 1127 (1975).
- <sup>35</sup>The energy gradient vectors of the two potential energy surfaces at the minimum of the seam of crossing (MSX) are parallel and are perpendicular to the tangent of the seam of crossing. See K. Kato, R. L. Jaffe, A. Komornicki, and K. Morokuma, *J. Chem. Phys.* **78**, 4567 (1983).